Theory of electron-phonon interactions on nanoscales: semiconductor surfaces and two dimensional electron gases

N. Buecking[a], S. Butscher[a], M. Richter[a], C. Weber[b], S. Declair[a], M. Woerner[c], K. Reimann[c], P. Kratzer[d], M. Scheffler[e] and A. Knorr[a]

[a]Institut für Theoretische Physik, Nichtlineare Optik und Quantenelektronik, Technische Universität Berlin, Hardenbergstr. 36, 10623 Berlin, Germany

[b]Mathematical Physics, Lund University, Box 118, 22100 Lund, Sweden

[c]Max Born Institut für Nichtlineare Optik und Kurzzeitspektroskopie, Max-Born-Straße 2A, 12489 Berlin, Germany

[d]Theoretische Physik, Universität Duisburg-Essen, Lotharstr. 1, 47048 Duisburg, Germany

[e]Fritz-Haber-Institut der Max-Planck-Gesellschaft, Faradayweg 4-6, 14195 Berlin, Germany

ABSTRACT

A theory of electron relaxation for electron gases in semiconductor quantum well structures and at semiconductor surfaces is presented. The electron relaxation is described by quantum-kinetic equations. In the nonlinear optical response of a two dimensional electron gas in a GaN quantum well, polaronic signatures are clearly enhanced compared to the linear response, if the pump pulse is tuned to the polaron energy. For the phonon-induced electron relaxation at Si (001) surface structures, the interplay of bulk and surface states yields a complex temporal relaxation dynamics depending on the slab thickness.

1. OUTLINE

After introducing the theoretical formalism for the underlying density matrix theory, we calculate in this paper the linear and nonlinear optical response of higher order electron-phonon interaction in ISB transitions in a GaN quantum well (QW) within a Bloch equation approach[1] using a correlation expansion[2,3] beyond the second order Born approximation. By generalizing such an approach beyond a single band problem,[4] our approach is able to qualitatively reproduce experimental results for doped gallium nitride quantum wells[5,6] in the linear and the nonlinear regime. In the last part of this paper, we investigate the relaxation dynamics at a silicon surface[7,8] after optical excitation. After performing density-functional-theory calculations for the Si (001) 2×1 surface, density matrix equations in the second order born limit are used to compute the evolution of the population of the conduction bands.[9,10]

2. THEORY OF THE ELECTRON-PHONON INTERACTION

Many-particle effects are of fundamental importance for the optical properties of two dimensionally quantum confined electrons in nanostructured semiconductors. Examples constitute finite free standing semiconductor slabs[9–12] as well as the ideal two dimensional electron gas (2DEG) in doped quantum wells.[13] The Hamilton operators of the free phonons and electrons, the electron-field interaction in dipole approximation and for the electron-phonon interaction are:[2,9]

$$\begin{aligned} H_0 &= \sum_{n\mathbf{k}} \varepsilon_{n\mathbf{k}} a^\dagger_{n\mathbf{k}} a_{n\mathbf{k}} + \sum_{i\mathbf{q}} \hbar\omega_{i\mathbf{q}} b^\dagger_{i\mathbf{q}} b_{i\mathbf{q}}, \qquad H_{\text{field}} = \sum_{\mathbf{k}n\neq n'} \mathbf{A}(t)\mathbf{p}^{n'\mathbf{k}}_{n\mathbf{k}}\, a^\dagger_{n\mathbf{k}} a_{n'\mathbf{k}}, \\ H_{\text{EPI}} &= \sum_{\substack{n\mathbf{k} \\ n'\mathbf{k}' \\ i\mathbf{q}}} g^{n'\mathbf{k}'}_{n\mathbf{k}\, i\mathbf{q}}\, a^\dagger_{n\mathbf{k}} a_{n'\mathbf{k}'} b_{i\mathbf{q}} + h.a.. \end{aligned} \tag{1}$$

Ultrafast Phenomena in Semiconductors and Nanostructure Materials XII
edited by Jin-Joo Song, Kong-Thon Tsen, Markus Betz, Abdulhakem Y. Elezzabi
Proc. of SPIE Vol. 6892, 689209, (2008) · 0277-786X/08/$18 · doi: 10.1117/12.768659

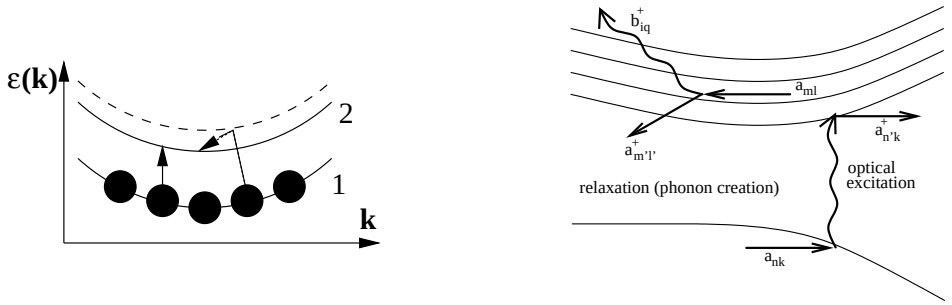

Figure 1. *Schematic diagram of the band structures and possible optical transitions. On the lhs, the left arrow indicates a single particle transition in a doped quantum well, where the lowest conduction subband is occupied. The right arrow indicates a transition via a virtual level, combined with a phonon emission process. On the rhs, excitation and electron relaxation in multiband-structure (band dispersion parallel to the surface) is illustrated.*

Here, $a^\dagger_{m\mathbf{k}}$, $a_{m\mathbf{k}}$ and $b^\dagger_{i\mathbf{q}}$, $b_{i\mathbf{q}}$ are creation and annihilation operators for electrons with wave vector $\mathbf{k}$ in (sub)band m and for phonons of mode i with wave vector $\mathbf{q}$ ($\mathbf{q}_{||}$ is its in-plane projection). $\varepsilon_{l\mathbf{k}}$ is the free energy of an electron in (sub)band l with wavevector $\mathbf{k}$ and $\omega_{i\mathbf{q}}$ the phonon frequency of a phonon in mode i at wave vector $\mathbf{q}$. With these operators, we can express coherences $p^{m\mathbf{l}}_{n\mathbf{k}} := \langle a^\dagger_{n\mathbf{k}} a_{m\mathbf{l}}\rangle$, (sub)band occupations $f_{n\mathbf{k}} := \langle a^\dagger_{n\mathbf{k}} a_{n\mathbf{k}}\rangle$, and the phonon occupation numbers $n_{i\mathbf{q}} = \langle b^\dagger_{i\mathbf{q}} b_{i\mathbf{q}}\rangle$. $g^{n'\mathbf{k}'}_{n\mathbf{k},i\mathbf{q}}$ denotes the electron-phonon coupling matrix elements, $\mathbf{p}^{m\mathbf{k}}_{n\mathbf{k}}$ is the momentum matrix element between (sub)band n and m, and $\mathbf{A}(t)$ the external electric vector potential describing the applied optical field.

Using the Heisenberg equation of motion we can find equations of motion (EOM) for the coherence and the phonon assisted density matrices $s^{m'\mathbf{l}'}_{m\mathbf{l},i\mathbf{q}} = \langle a^\dagger_{m\mathbf{l}} a_{m'\mathbf{l}'} b_{i\mathbf{q}}\rangle$:[9]

$$
\begin{aligned}
i\hbar\frac{d}{dt}p^{m'\mathbf{l}'}_{m\mathbf{l}} =& \left(\varepsilon_{m\mathbf{l}} - \varepsilon_{m'\mathbf{l}'}\right)p^{m'\mathbf{l}'}_{m\mathbf{l}} + \mathbf{A}(t)\sum_{n\mathbf{k}}\left(\mathbf{p}^{n\mathbf{k}}_{m\mathbf{l}}p^{m'\mathbf{l}'}_{n\mathbf{k}} - \mathbf{p}^{m'\mathbf{l}'}_{n\mathbf{k}}p^{n\mathbf{k}}_{m\mathbf{l}}\right) \\
&+ \sum_{\substack{n\mathbf{k}\\ i\mathbf{q}}}\left(g^{n\mathbf{k}}_{m\mathbf{l}\,i\mathbf{q}}\left(s^{n\mathbf{k}}_{m'\mathbf{l}'\,i\mathbf{q}}\right)^* + g^{n\mathbf{k}}_{m\mathbf{l}\,i\mathbf{q}}s^{m'\mathbf{l}'}_{a_{n\mathbf{k}}\,i\mathbf{q}} - g^{m'\mathbf{l}'}_{n\mathbf{k}\,i\mathbf{q}}\left(s^{m\mathbf{l}}_{n\mathbf{k}\,i\mathbf{q}}\right)^* - g^{m'\mathbf{l}'}_{n\mathbf{k}\,i\mathbf{q}}s^{n\mathbf{k}}_{m\mathbf{l}\,i\mathbf{q}}\right)
\end{aligned}
\tag{2a}
$$

and

$$
\begin{aligned}
i\hbar\frac{d}{dt}\left(s^{m\mathbf{l}}_{m'\mathbf{l}'\,i\mathbf{q}}\right)^* =& \left(\varepsilon_{m\mathbf{l}} - \varepsilon_{m'\mathbf{l}'} + \hbar\omega_{i\mathbf{q}}\right)\left(s^{m\mathbf{l}}_{m'\mathbf{l}'\,i\mathbf{q}}\right)^* + \mathbf{A}(t)\sum_{n\mathbf{k}}\left(\mathbf{p}^{n\mathbf{k}}_{m\mathbf{l}}\left(s^{n\mathbf{k}}_{m'\mathbf{l}'\,i\mathbf{q}}\right)^* - \mathbf{p}^{m'\mathbf{l}'}_{n\mathbf{k}}\left(s^{m\mathbf{l}}_{n\mathbf{k}\,i\mathbf{q}}\right)^*\right) \\
&+ \sum_{\substack{n\mathbf{k}\\ i'\mathbf{q}'}}\left(g^{n\mathbf{k}}_{m\mathbf{l}\,i'\mathbf{q}'}\left(R^{m'\mathbf{l}'}_{n\mathbf{k}\,i\mathbf{q}}\right)^* + g^{n\mathbf{k}}_{m\mathbf{l}\,i'\mathbf{q}'}T^{m'\mathbf{l}'}_{n\mathbf{k}\,i\mathbf{q}} - g^{m'\mathbf{l}'}_{n\mathbf{k}\,i'\mathbf{q}'}\left(R^{n\mathbf{k}}_{m\mathbf{l}\,i\mathbf{q}}\right)^* - g^{m'\mathbf{l}'}_{n\mathbf{k}\,i'\mathbf{q}'}T^{n\mathbf{k}'}_{m\mathbf{l}\,i\mathbf{q}}\right) \\
&+ \sum_{\substack{n\mathbf{k}\\ n'\mathbf{k}'}} g^{n'\mathbf{k}'}_{n\mathbf{k}\,i\mathbf{q}}\langle a^\dagger_{m\mathbf{l}}a^\dagger_{n\mathbf{k}}a_{m'\mathbf{l}'}a_{n'\mathbf{k}'}\rangle,
\end{aligned}
\tag{2b}
$$

where $R^{m\mathbf{l},i'\mathbf{q}'}_{n\mathbf{k},i\mathbf{q}} = \langle a^\dagger_{n\mathbf{k}}a_{m\mathbf{l}}b_{i\mathbf{q}}b_{i'\mathbf{q}'}\rangle$ and $T^{m\mathbf{l},i'\mathbf{q}'}_{n\mathbf{k},i\mathbf{q}} = \langle a^\dagger_{n\mathbf{k}}a_{m\mathbf{l}}b^\dagger_{i\mathbf{q}}b_{i'\mathbf{q}'}\rangle$. Through the electron-phonon interaction, the resulting equations of motion[9,14,15] (Eqs. (2a), (2b)) of the single particle density matrices $p^{m'\mathbf{l}'}_{m\mathbf{l}}$ couple to phonon assisted density matrices $s^{m\mathbf{l}}_{m'\mathbf{l}',i\mathbf{q}}$, which in turn couple to higher order interaction matrices $R^{m\mathbf{l},i'\mathbf{q}'}_{n\mathbf{k},i\mathbf{q}}$, $T^{m\mathbf{l},i'\mathbf{q}'}_{n\mathbf{k},i\mathbf{q}}$ and $\langle a^\dagger_{m\mathbf{l}}a^\dagger_{n\mathbf{k}}a_{m'\mathbf{l}'}a_{n'\mathbf{k}'}\rangle$. In order to get a closed set of equations of motion, we truncate the resulting hierarchy, using a correlation expansion.[2]

2.1 Quantum kinetics

For larger couplings of the electron-phonon interaction as in GaN, a second Born approximation (theory in g^2) fails and higher order interactions (in g^n) need to be included, in particular two particle correlations such as

$R^{m\mathbf{l},i'\mathbf{q}'}_{n\mathbf{k},i\mathbf{q}}$ and $T^{m\mathbf{l},i'\mathbf{q}'}_{n\mathbf{k},i\mathbf{q}}$. A full dynamical treatment of such quantities is very involved. Therefore the two-particle correlations R and T are treated in Markov approximation, while keeping the full non-Markovian dynamics of the s matrices. This scheme was introduced for the scattering dynamics in a single band.[4] Besides the first order contributions to the equations of motion published in Ref.,[14] the higher order contributions (HO) to the phonon-assisted density matrices read:

$$\frac{d}{dt} s^{n'\mathbf{k}'}_{n\mathbf{k}\atop i\mathbf{q}}|^{HO} = -\left(\Gamma^{\text{in}}_{n'\mathbf{k}'} + \Gamma^{\text{out}}_{n'\mathbf{k}}\right) s^{n'\mathbf{k}'}_{n\mathbf{k}\atop i\mathbf{q}} \tag{3}$$

where the scattering rates Γ are defined as

$$\begin{aligned}
\Gamma^{\text{in}}_{n'\mathbf{k}'} =& \frac{\pi}{\hbar} \sum_{\mathbf{k}'\mathbf{q}\pm} \left| g^{n'\mathbf{k}'}_{n\mathbf{k}\atop i\mathbf{q}} \right|^2 \delta(\epsilon_{n\mathbf{k}} - \epsilon_{n'\mathbf{k}'} \pm \hbar\omega_{i\mathbf{q}})(n_{\mathbf{q}} + \frac{1}{2} \pm \frac{1}{2}) f_{n'\mathbf{k}'} \\
\Gamma^{\text{out}}_{n'\mathbf{k}'} =& \frac{\pi}{\hbar} \sum_{\mathbf{k}'\mathbf{q}\pm} \left| g^{n'\mathbf{k}'}_{n\mathbf{k}\atop i\mathbf{q}} \right|^2 \delta(\epsilon_{n\mathbf{k}} - \epsilon_{n'\mathbf{k}'} \pm \hbar\omega_{i\mathbf{q}})(n_{\mathbf{q}} + \frac{1}{2} \mp \frac{1}{2})(1 - f_{n'\mathbf{k}'}).
\end{aligned} \tag{4}$$

A detailed derivation of these equations can be found in Ref.[16] Obviously, within the used self-consistent Born approximation microscopically determined lifetime contributions Γ, Eq. (4), occur for the phonon-assisted density matrices.

2.2 Markovian dynamics

If we apply a second order Born approximation within a Markovian limit ($\Gamma \to 0$) and a bath hypothesis to the equations of motion (2a) and (2b), we obtain equations of the form[2,9]

$$\frac{d}{dt} f_{n\mathbf{k}} = -2 \sum_{n'} \left(\Gamma^{\text{in}}_{n'\mathbf{k}} f_{n\mathbf{k}} + \Gamma^{\text{out}}_{n'\mathbf{k}} (1 - f_{n\mathbf{k}}) \right). \tag{5}$$

In a weak coupling regime and weak excitation, these EOM are sufficient to describe the relaxation dynamics.

2.3 Single particle energies

For the modelling of the intersubband structure of the quantum wells a parabolic band approximation within the effective mass concept can be used for the single particle energies $\epsilon_{n\mathbf{k}}$. This concept generally fails for more complex two dimensional systems like a surface structure. While for a bulk structure, simplifying assumptions for the electronic band structure are often possible, the dynamics of excited electrons at a surface structure is usually dominated by the interplay of bulk electrons and additional surface induced bands. Consequently, a precise knowledge of the electronic band structure is necessary for the accurate description of dynamical processes in such a structure. We show that a possible approach to calculate the relaxation dynamics in this field is to combine *density-functional theory (DFT)* for the calculation of the electronic band structure and the interaction matrix parameters $g^{n'\mathbf{k}'}_{n\mathbf{k},i\mathbf{q}}$ with a *density-matrix (DMT)* approach to derive dynamical equations.

3. OPTICAL RESPONSE OF A DOPED GALLIUM-NITRIDE QUANTUM WELL

Recent studies have investigated the linear optical response of doped quantum well systems with special emphasis on intersubband (ISB) transitions in the conduction band.[17,18] In particular, it was shown in Ref.[14] that a non-Markovian treatment of the electron-phonon interaction in the weak coupling regime reveals polaron signatures in absorption, e.g. phonon satellites spectrally located around the Huang Rhys shifted subband gap. A similar behavior is known from two level systems, like interband transitions of a semiconductor quantum dot, where the independent boson model provides an analytic solution.[19–21] Such exact solutions, which are valid in all coupling regimes, do not exist for a two subband system in two dimensions, in contrast to one dimensional systems where linear absorption was investigated in detail.[22] Nevertheless, a time-convolutionless density matrix approach has been used successfully to calculate the non-perturbative effects of the electron-phonon interaction for the linear absorption spectrum of ISB transitions in GaN quantum wells,[23] including polaron satellites of arbitrary order. Unfortunately, this non-perturbative approach is not suitable for non-linear optical excitations.

3.1 Linear absorption

To characterize the doped quantum well used to describe the nonlinear response, we consider the linear absorption spectrum of the ISB transition in a GaN QW, shown in Fig. 2. The absorption is calculated using $-\ln T = \alpha L$ with $L = 6$nm assumed for the calculation and α is calculated using:

$$\alpha_0(\omega) = \frac{\omega}{cn(\omega)} \mathrm{Im}\left(\frac{P(\omega)}{\varepsilon_0 E(\omega)}\right). \tag{6}$$

Here, the dipole density reads $P(t) := \sum_{n,n',\mathbf{k}} \frac{1}{\omega_0} \mathbf{e} \mathbf{p}^{n'}_{n\mathbf{k}} p^{n}_{n'\mathbf{k}}(E(t))$, where ω_0 and $\mathbf{e}$ are the frequency and polarization of the incident light field $E(t)$. The considered ISB transition has a gap energy of 270 meV and a carrier density of $10^{13}\mathrm{cm}^{-2}$. All calculations are carried out at room temperature using Eq. (4) and equations of motion of Ref.[14] including the contribution from Eqs. (3) and (4). Matrix elements are calculated in Ref.[23], where all material parameters can be found. Fig. 2 shows, that the electron-phonon interaction (solid line) introduces a considerable polaron shift of 20 meV, the maximum of the absorption (zero phonon peak) is found at 250 meV. Due to scattering with phonons, we also observe a strong broadening of the ISB transition towards higher energies, well known from previous calculations with the time convolutionless theory.[23] The qualitative agreement with experimental data (dotted line from Ref.[5]) considering the unusually long absorption tail towards higher energies is good, but yet our calculations reveal a clearly smaller line width of the main resonance (solid line). This is not surprising, since other line broadening mechanisms, effectively acting on the zero phonon line width have not been considered. Interaction with impurities or strain effects may explain this discrepancy. These effects are not the topic of the paper. If we introduce an additional phenomenological dephasing of the intersubband coherence, with a time constant of γ (dashed lines in Fig. 2), the agreement for the zero phonon peak line width can be improved, while this has no impact the absorption tail on the high energy side, which is the focus of this paper (Sec. 3.2). An improvement of γ seems to reduce the oscillator strength in the visible range, since the increased line shape width leads to an redistribution of oscillator strength out of the plotted energy range. The broad absorption peak arising through the electron-phonon interaction (see curves labeled 10 meV-40 meV in Fig. 2), does not yield deeper insight into the many-particle physics of the electron-phonon interaction. Therefore, we consider the nonlinear optical response of the high energy part absorption tail.

3.2 Nonlinear optics: pump-probe spectra

We consider a non-linear optical excitation during a 100 fs pulse that has a center frequency of 355 meV (first phonon resonance, cf. Fig. 2) and an intensity of 9.6 GWcm $^{-2}$. Such an excitation transfers about 6 % of the ground state carrier density into the upper subband. The calculated differential transmission:[24]

$$DTS(\omega) = \frac{\Delta T(\omega)}{T_0(\omega)} = \frac{e^{\alpha_{PP}(\omega)L} - e^{\alpha_0(\omega)L}}{e^{\alpha_0(\omega)L}} = e^{[\alpha_{PP}(\omega) - \alpha_0(\omega)]L} - 1, \tag{7}$$

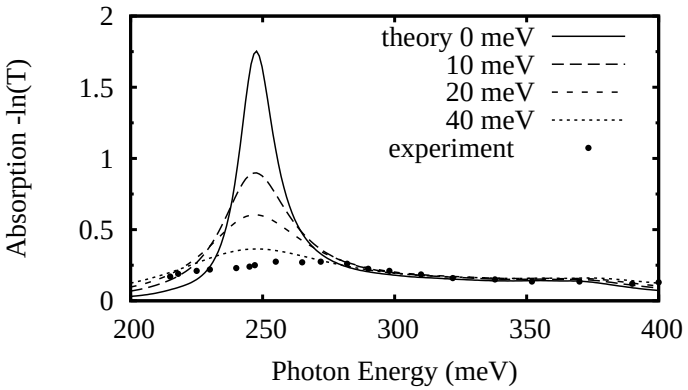

Figure 2. *Linear absorption spectra of a GaN QW at 300 K, theoretical calculation including the interaction with LO-phonons (solid line) and with additional phenomenological dephasing γ of 10, 20, and 40 meV/ħ (dashed lines) and experimental data from.*[5]

is shown in Fig. 3 (solid lines) for different time delays τ between pump and probe pulse. Data (experimental details can be found in Ref.[5]) are shown as dots. A detailed derivation of the formula for α_{pp} is given in Ref.,[25] only the ω-dependence is not neglected in this treatment, so that the ω dependent prefactors are kept (cf. the linear case Eq. (6)). Especially for negative delay times (probe before pump, see Fig. 3 a), we obtain a dispersive signature around the single particle transition energy, due to the off-resonant excitation (Stark effect).[26] The position of the resonance has to be identified with the zero crossing at 250 meV. One phonon energy above the single phonon energy (355 meV) we find a resonant signature in the DTS spectra, which shows a very similar behavior in theory and experiment and decays rapidly after the excitation.[5] This signature is caused by the dynamical Stark effect during the overlapping pulses. Only a non-Markovian treatment of the EPI can reveal this effect, while a Markovian theory fails in second order Born approximation (not shown).

The theoretical results show deviations, in particular line shifts, from the experiment around the zero phonon line at 250 meV. We attribute these deviation to similar processes discussed for the linear absorption, Sec. 3.1, like Coulomb effects or strain induced effects. In particular, electron localization effects in the plane of the well may resemble to a more level like response[5] in comparison to the bulk response shown here. Our main point is to show that the phonon replica at 355 meV is clearly enhanced in nonlinear (Fig. 3) in comparison to the linear spectroscopy (Fig. 2).

One might wonder, why the energetic distance between the two resonant signatures is not exactly equal to the phonon energy like it was with the two level assumption in.[5] We attribute the reason for this to the electronic dispersion inside the quantum well subband: With the resonant excitation at the first phonon side band, a part of the polaronic states connected to electron distribution in the subband are mostly resonantly excited, nevertheless these states have a less effective dipole moment than the main peak (cf. Fig 2). Additionally, the electrons inside the subbands that cause the main linear absorption peak are non-resonantly excited, where the excitation strength is determined by their dipole moment and the invidual detuning. Such effects cannot occur in a two level system system and are specific to the two subband system.

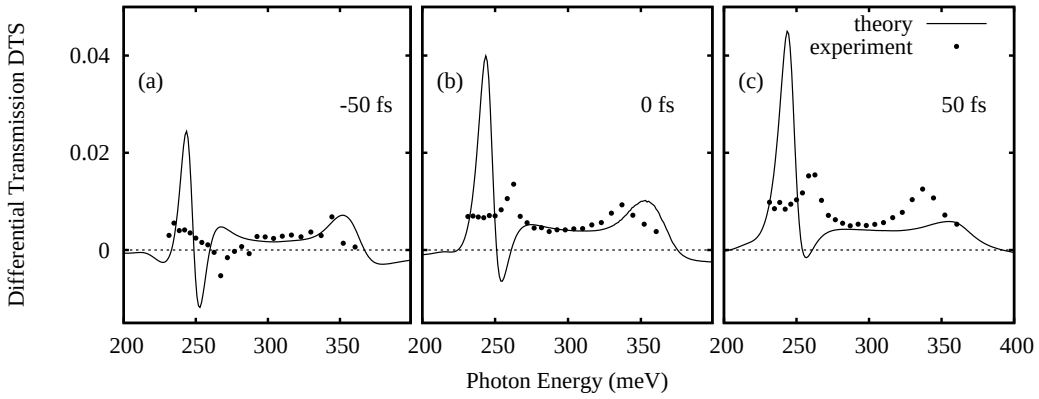

Figure 3. *DTS spectra at different delay times (a) -50 fs, (b) 0 fs, (c) 50 fs. The sample is nonlinearly excited with a second 100 fs pulse at the first phonon replica around 355 meV.*

4. RELAXATION DYNAMICS AT THE SILICON (001) 2×1 SURFACE

Electron relaxation phenomena at silicon surfaces are a topic of recent research.[27,28] A characteristic detail of the silicon (001) surface is the reconstruction incorporating a tilted dimer.[7,8] In the band structure, this feature results in the formation of additional surface bands located partly inside the semiconductor bandgap.[9] These surface bands (D^{up} and D^{down})are related to the p-orbitals of the dimer atoms.[8] While the D^{up} band is a valence band, the D^{down} band is not populated at zero temperature. In experimental studies,[27,28] it has been found that the phonon-induced relaxation inside the conduction bands is a complex process on multiple timescales. The interplay of interband scattering from the bulk to the D^{down} band and intraband scattering inside the D^{down} bands are found to be the dominating processes. In this section, we use the Markovian dynamical equations (5) to

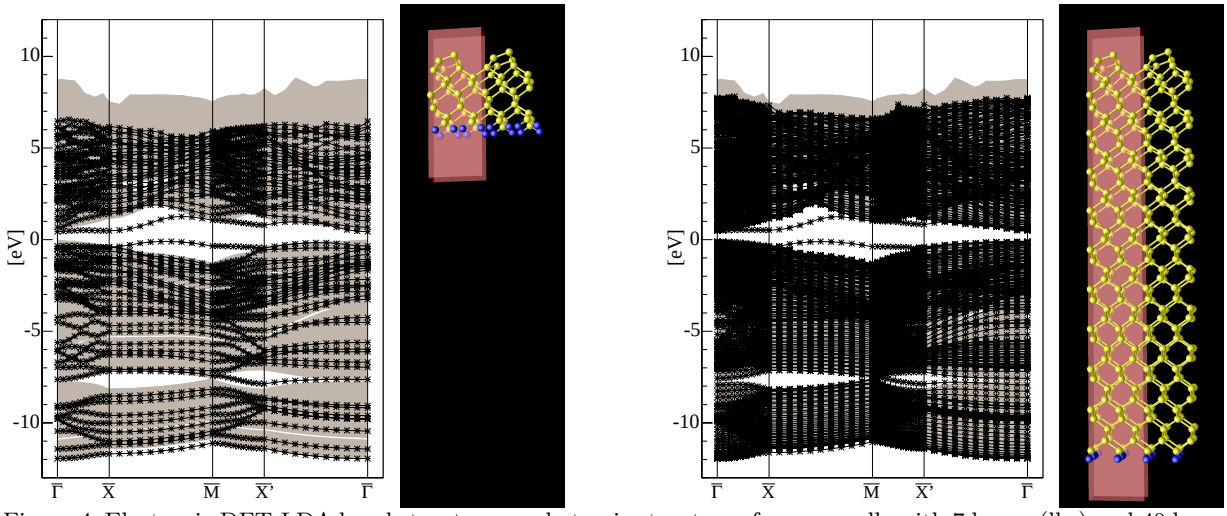

Figure 4. Electronic DFT-LDA band structures and atomic structures for supercells with 7 layers (lhs) and 40 layers (rhs). Besides the bulk-related bands (grey shaded regions), the D^{up} and D^{down} bands are observable in the band gap.

calculate the population dynamics at the Silicon 2×1 surface, while the surface bandstructure and wave functions calculated preliminarily by DFT.[29]

4.1 Linking density-functional theory and density-matrix theory

Phonon induced relaxation dynamics at the silicon (001) surface is investigated in terms of a two-step model. In a first step, the electronic structure of the surface structure is computed using DFT within the local-density approximation (LDA).[30] The calculation is performed in the supercell-approach,[9] with a reconstruction of 3 layers at the surface, while at the other end of the structure, the chemical bonds are saturated by hydrogen atoms. The implementation of the DFT computer code uses plane-wave-basis set and pseudopotentials. In the second step, the population dynamics is calculated using the results of the first (DFT) step by DMT in the Markovian limit.

DFT: In Fig. 4, the electronic band structures are shown for supercells of 7 layers and 40 layers. The atomic positions and the size of the supercell are plotted by a ball-and-stick model for those two structures. The number of bulk-bands is highly dependent on the number of layers in the calculation, and for a reasonable sampling of the band structure, obviously a fairly thick slab ($\gg$ 20 layers) is needed to model the bulk effects of a single surface. Due to the description of the bandstructure within DFT-LDA, the semiconductor band-gap is underestimated by ca. 0.52 eV with respect to the experimentally provided values.[10,30] As the electron dynamics is only investigated for the conduction bands by our approach and this shift of the band-gap energy is mostly independent of the $\mathbf{k}$-location, this effect has no big influence on the conduction band structure and it is a good approximation to use the Kohn-Sham eigenvalues of the DFT-LDA calculation for the further discussion of the dynamics.

DMT: The electronic structure from the DFT calculations is now used to perform calculations on the electron population dynamics of the conduction band states using Eq. (5). Using Kohn-Sham eigenvalues from the DFT-LDA calculation (step 1), the properties of the silicon surface enter into these equations of motion via the electron field interaction $\mathbf{p}_{n\mathbf{k}}^{m\mathbf{k}}$ (momentum matrix elements) and the electron-phonon coupling parameters:

$$g_{n\mathbf{k},i\mathbf{q}}^{n'\mathbf{k}'} = g_{i\mathbf{q}} \sum_{\mathbf{G},\mathbf{G}'} u_{n\mathbf{k}}^{*}(\mathbf{G}) u_{n'\mathbf{k}'}(\mathbf{G}') \delta_{\mathbf{k}+\mathbf{G},\mathbf{k}'+\mathbf{G}'+\mathbf{q}}. \tag{8}$$

Here, $u_{m\mathbf{k}'}(\mathbf{G}')$ represent electronic Bloch waves in the $\mathbf{k}$-space representation (Fourier transform of the real space representation). Through the inhomogeneous delta condition in this equation (where the $\mathbf{k}$ vectors are not generally decoupled from the reciprocal lattice vectors $\mathbf{G}$), a scattering over the Brillouin zone boundary can be

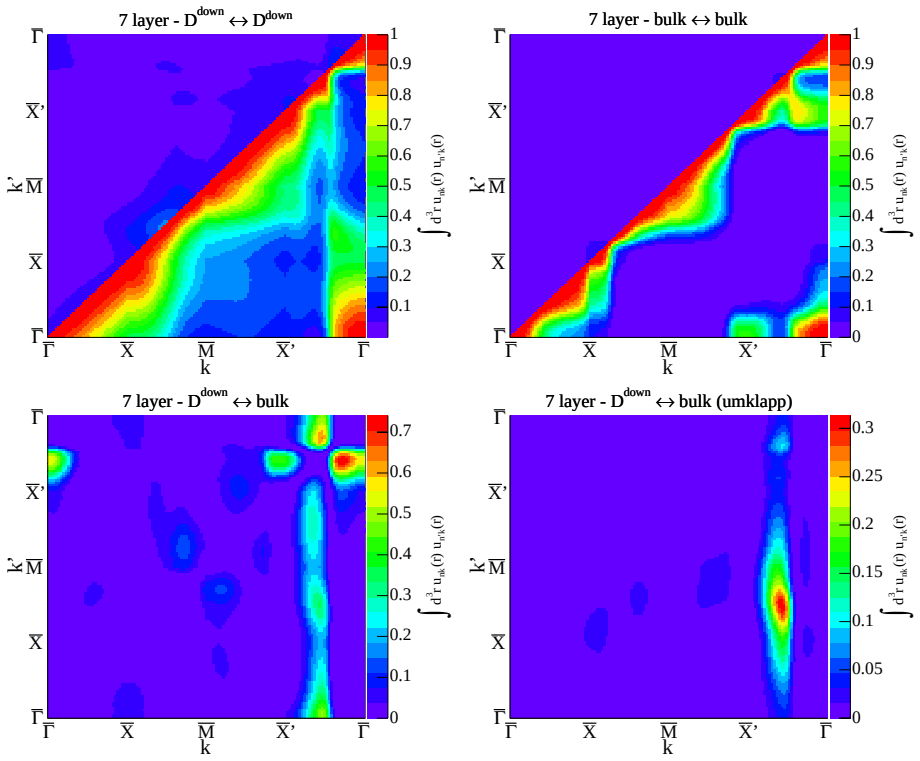

Figure 5. Square modulus of the electron matrix elements for different transitions. Top row: intraband transitions, inside D^{down} band (lhs) and inside lowest bulk conduction band (rhs), bottom row: interband transition from D^{down} band to first bulk band (lhs) and corresponding umklapp process via zone boundary. The transition are shown for a transition from an an initial state to a final state on the symmetry line.

described. For small $\mathbf{k}$ and $\mathbf{q}$ however, the general delta condition falls back to the commonly used momentum conservation condition $\mathbf{k} = \mathbf{k}' + \mathbf{q}$.

While the phonon-mode dependent coupling parameter $g_{i\mathbf{q}}$ is approximated by typical values from bulk silicon,[31] the part $I_{n\mathbf{k}}^{n'\mathbf{k}'} = \sum_{\mathbf{G},\mathbf{G}'} u_{n\mathbf{k}}^*(\mathbf{G}) u_{n'\mathbf{k}'}(\mathbf{G}')$ depends on the electronic wave functions of the underlying structure. Here, the *Kohn-Sham* wave functions are used to calculate the electron-state dependent transition amplitudes for all involved bands. In Fig. 5, the modulus of the transition integrals $I_{n\mathbf{k}}^{n'\mathbf{k}'}$ of the electronic wave functions is depicted. For the intraband transitions (top row of Fig. 5), the modulus approaches a value of 1 on the diagonal ($\mathbf{q} = 0$, initial and final states are the identical). Furthermore, for intraband scattering, the modulus remains unchanged with respect to the exchange of inital and final states, and in place of the corresponding symmetrical representation, an umklapp process is plotted in the upper left half of the top row pictures in Fig. 5. It is obvious that the scattering via umklapp process is only of minor importance for this intraband scattering (one order of magnitude less than via direct scattering). For the interband processes (bottom row of Fig. 5), scattering is limited to some specific points within the Brillouin zone (here, scattering on the diagonal is always vanishing, as initial and final states are orthogonal for different bands at the same $\mathbf{k}$-point). Furthermore, the umklapp-scattering (rhs of the bottom row of Fig. 5) now differs only by a factor of 3 from the direct processes. As a consequence, we cannot generally neglect the scattering over the Brillouin zone boundary. We note that these considerations are focused on one part of the electron-phonon scattering processes ($I_{n\mathbf{k}}^{n'\mathbf{k}'}$), while the phonon mode dependent form factor $g_{i\mathbf{q}}$ and scattering in the equations of motion Eq. (5) is highly dependent on the wave number $\mathbf{q}$ as the scattering matrices (4) contain the energy conservation for the scattering processes. In the numerical simulation of Eq. (5), all these effects are taken into account.

The discussion of the involved electron-phonon interaction induced relaxation dynamics is investigated using Eq. (5). The initial population in this approach is provided by simulating the linear absorption of a finite-

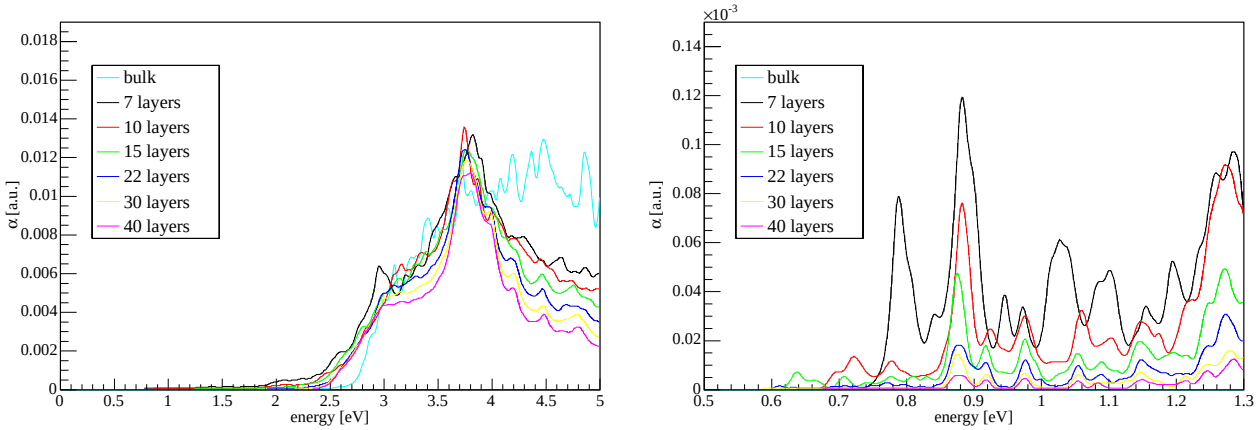

Figure 6. Linear absorption spectra for the Si 2×1 (001) surface for different supercell structures and for the bulk. On the rhs, a cutout of the full spectrum at the lhs is shown.

length optical pulse without considering the interference of the optically induced electron preparation with the relaxation dynamics.

4.2 Linear spectra

The linear spectrum of the silicon 2×1 surface can be calculated according to Eq. (6). In Fig. 6, linear spectra are shown for a variety of supercells with increasing slab thickness. Within these plots, only the direct optical transitions (via the matrix elements $p_{n\mathbf{k}}^{n'\mathbf{k}}$, Eq. (1)) are considered, while indirect optical scattering and relaxation processes are neglected. On the lhs of Fig. 6, the spectrum is shown in the range from 0 eV to 4 eV. While significant differences are observable for the different surface supercells the onset of the bulk spectrum is only visible above 2.7 eV (due to the indirect bandgap of silicon), while there are pronounced contributions to the surface spectra at lower energies (2.0 - 2.5 eV). These additional transitions in the spectrum are related to the D^{down} surface band in the band structure (Fig. 4). In the cut of the spectrum (rhs of Fig. 6) for the range of 0.5-1.3 eV, all visible peaks are related to transitions from the valence bands to the D^{down} band. Due to the scissors shift (cf. Sec. 4.1), the optical pulse used for the simulation of the relaxation dynamics corresponds to a pulse of 1.07 eV in the DFT-LDA bandstructure.

The initial population for the relaxation dynamics discussed in the next section is consequently induced by some of the peaks in Fig. 6 (rhs). Furthermore, the position of some the peaks differs in this figure between the slabs (the height of the peaks is decreased with increasing layer number due to a volume-surface effect). As a consequence, for the simulation of optical excitation in the very narrow energy range of 0.5-1.3 eV, a big layer number is obviously needed.

4.3 Relaxation dynamics

The evolution of the population of the conduction band states is shown in Fig. 7 for two supercells of 7 (lhs) and 40 layers (rhs). At top level, the corresponding conduction band structure is depicted, where the zero of the energy axis corresponds to the minimum of the D^{down} band (the leftmost bands in the two bandstructure pictures in Fig. 7). The inital occupation[10]

$$f_{n\mathbf{k}}^{\text{initial}} = \frac{1}{\hbar^2} \sum_m \left| \mathbf{p}_{n\mathbf{k}}^m \widetilde{A}\Big(\frac{\epsilon_{m\mathbf{k}} - \epsilon_{n\mathbf{k}}}{\hbar} \Big) \right|^2 \tag{9}$$

with the Fourier-transform optical vector potential $\widetilde{A}(\omega)$ is calculated for an optical pulse of 1.69 eV (corresponding to 1.07 eV in the LDA-bandstructure) and 100 fs duration. Only a few bands are located in the relevant optical excitation energy range which can be populated: For the 7-layer slab, the entire relaxation process extends on 2 bands (the D^{down} and one bulk band), for the 40-layer slab, about 10 bands are in the "active region".

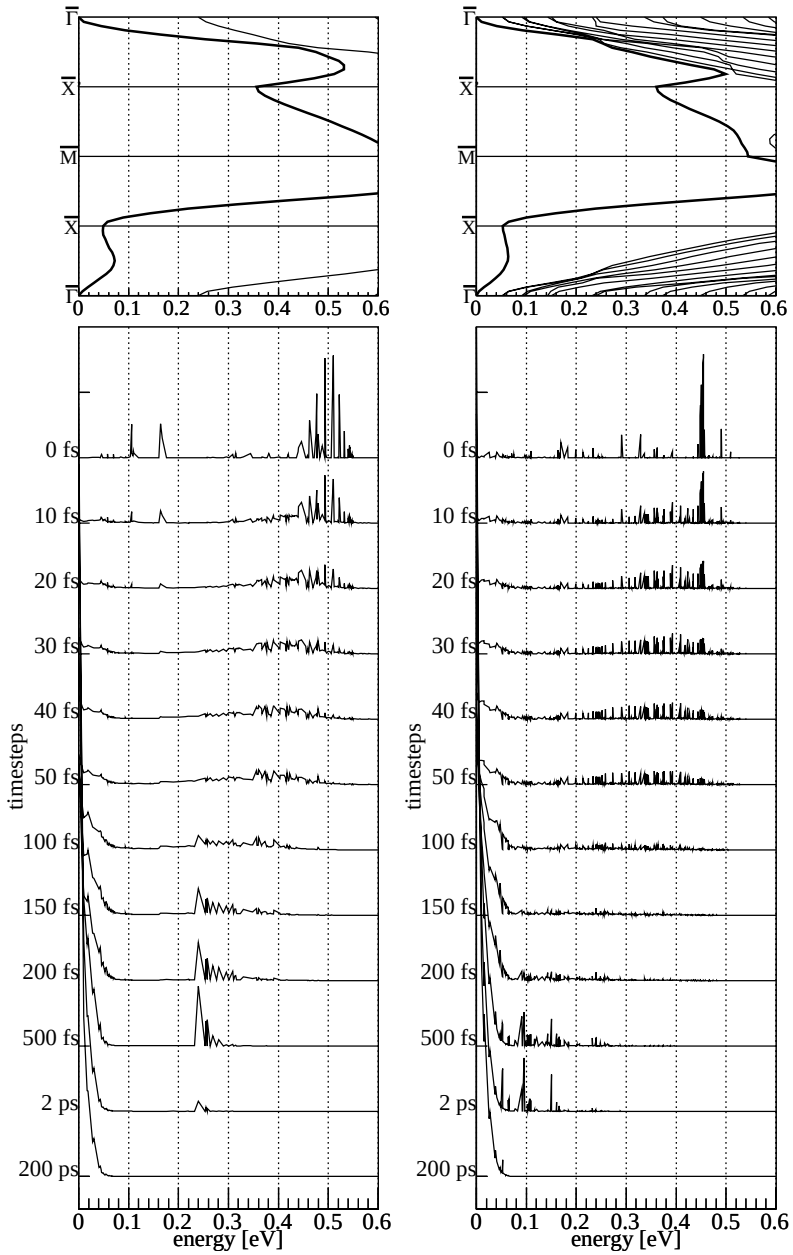

Figure 7. Relaxation dynamics after initial excitation with optical initial conditions for a slab of 7 layers and 40 layers.

In both calculations, the major part of the initial population is located within a few states at about 0.46 eV, but the energetical localization is much narrower in the 40 layer calculation. By projection to real space (Fig. 8), it can be seen that this initial population is almost completly inside the surface band, while the bulk band(s) are not strongly populated by the optical excitation.

It is clearly visible in Fig. 7 (bottom) that the relaxation processes out of a non-equilibrium initial situation to a quasi-equilibrium final state happens on multiple timescales and includes the whole energy scale of the energy dispersion. The shape of the initial distribution is dispersed fast (30 fs), and after 50 fs, a significant population of the conduction band minimum is found. While this fast timescales do not differ for the two supercells, larger differences can be found after 100 fs: for the 7-layer supercell, a strong population forms at the energetic position

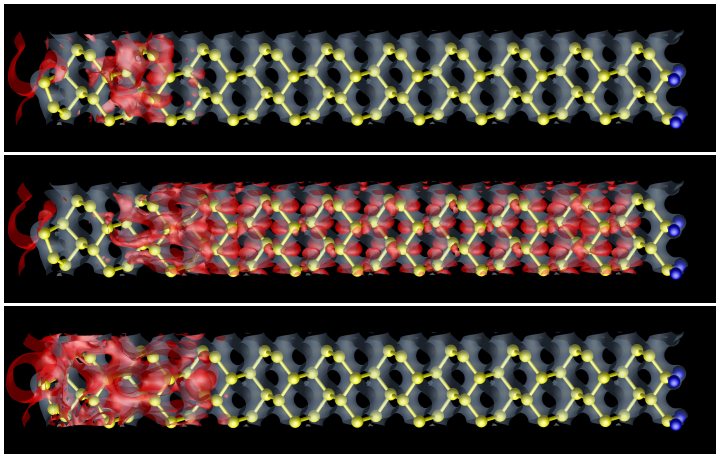

Figure 8. Projection of the conduction band population into the real space for timesteps of 0, 2 and 190 ps. While the initial population is strongly localized at surface, the population partly shifts to the bulk at 2 ps, and finally returns into a surface state (minimum of D^{down}-band).

of the (single) bulk band minimum (0.24 eV), reaching its maximum at 500 fs and is almost gone after 2 ps. At this timestep, the rest of the population already resembles a fermi distribution at the conduction band minimum. For the 40-layer supercell, the lowest bulk band minmum is at 0.08 eV, and a local population maximum forms at 0.08-0.1 eV. Both the formation time of this population accumulation and the decay time are much longer than for the 7-layer case: the maximum is reached at about 2 ps, and some minor peaks are still present at 200 ps relaxation time. As an obvious conclusion, we can see that the relaxation highly depends on the slab thickness leading to a electronic band structure in the involved energetic region relevant for the relaxation processes (and thus the representation of the supercell with only a few layers is insufficient to calculate the relaxation process).

By comparing this specific relaxation behaviour (Fig. 7) in the real-space representation (Fig. 8), it can be seen that the slower relaxation processes (2 ps) are obviously related to a population of the bulk bands (after the initial preparation at the surface) and a subsequent backscattering to the surface state (the conduction band minimum of the surface band structure is in the D^{down}-band). A qualitative explanation of the involved processes is that the intra-surface-scattering is much stronger than the bulk-scattering due to the difference in the strength of the related matrix elements (cf. Fig. 5). A more quantitative discussion of the relaxation will be done in the next paragraph. In any case, the relaxation via the bulk states is an alternative (but slow) relaxation channel to the direct intraband relaxation inside the surface band.

The dependence of the relaxation times on the supercell thickness can be investigated by an examination of the population of the conduction band minimum (which is also the minimum of the D^{down} band). In Fig. 9, the time-dependent population of the state representing the minimum is drawn on a logarithmic timescale. Two timescales can be clearly identified (lhs of Fig. 9): At the beginning of the relaxation (t <1 ps), the state is populated with on a ps-timescale. At the end of relaxation (middle of Fig. 9), a much slower timescale highly sensitive to the supercell size applies. The dashed lines refer to the exponential fit functions to extract numerical values for the timescales. Those extracted timescales are visualized in Fig. 9 (rhs) for different supercells on a logarithmic scale: While the short-term time-scale remains close to the 1 ps relaxation time for all different supercells, the long-term timescale varies from 2.5 ps (7-layer slab) to 60.0 ps (40-layer slab), where a thicker slab generally leads to a slower relaxation. This can by explained by the interplay of the scattering via electron-optical and -acoustical phonons: The intraband scattering inside the surface band is always dominated by optical phonons due to the fairly strong bending of the band in the $\overline{X}-\overline{M}$-direction. The same explanation applies for the scattering from the surface-band to bulk states. The character of the scattering from bulk to surface for a specific supercell, however, depends strongly on the actual position of the bulk bands in the band structure (Fig. 4): while for 7 bands, an energetical gap of 0.2 eV between the lowest bulk band and the minimum of the D^{down}-band is observable, this gap is only about 0.01 eV for the 40 layer slab. As a consequence, for 7 layers,

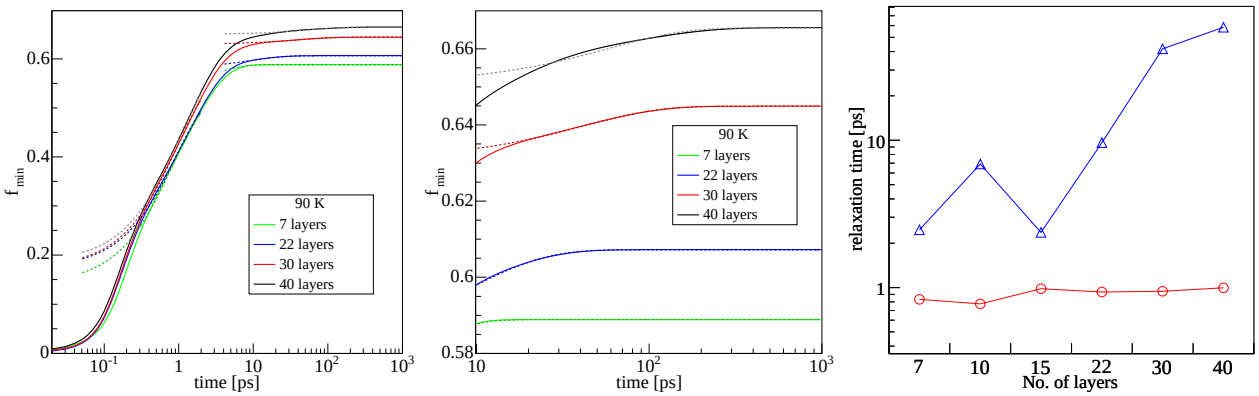

Figure 9. Relaxation timescales of the Si 2×1 surface for different supercells. On the lhs, the population of the conduction band minimum (D^{down}-band) is shown on a logarithmic timescale. In the middle column, a cutout of this population dynamics is drawn for times gt. than 10 ps. On the rhs, the relaxation timescales extracted from the lhs. data is shown for the different supercells.

also bulk-surface scattering is dominated by optical scattering, whereas for 40 layers only acoustical phonons allow to override the small energy gap. As the optical phonons are both coupled by a much stronger deformation potential (5× stronger than for acoustical phonons) to the electrons and the energy transfer per scattering event is bigger for optical phonons, the typical relaxation times for an optical-phonon mediated scattering are much faster than for acoustical scattering.

5. CONCLUSION

We have reviewed a theory for the description phonon-induced relaxation phenomena in two dimensional systems. By applying this theory to nonlinear optical properties of phonon assisted intersubband transitions in GaN including the non-Markovian nature of the electron-phonon interaction, our numerical calculations agree qualitatively with recent experimental work[5] and shows a satellite peak due to LO electron-phonon interaction, which is clearly visible only in nonlinear pump probe spectra. Our conclusion is that pump probe spectroscopy is appropriate to uncover non-Markovian polaron effects, that are not visible in linear spectra. The investigation of phonon induced relaxation at the silicon 2×1 (001) surface reveals a complex relaxation process on two timescales involving surface-surface and bulk-surface scattering. The timescales are in agreement to experimental findings recently published[28] and the different magnitude can be related to optical phonon scattering inside the D^{down}-surface band for the fast timescale and acoustical phonon scattering for the slower processes from the bulk to the surface band.

The authors acknowledge financial support by the Deutsche Forschungsgemeinschaft through KN 427 4-1, KN 427 3-1, SPP 1093, Sfb 787 and the CoE UniCat.

REFERENCES

1. M. Lindberg and S. W. Koch, "Effective bloch equations for semiconductors," *Phys. Rev. B* **38**, pp. 3342–3350, Aug 1988.
2. T. Kuhn, *Theory of Transport Properties of Semiconductor Nanostructures*, ch. 6, p. 173. Chapman & Hall, London, 1998. edited by E. Schöll.
3. F. Rossi and T. Kuhn, "Theory of ultrafast phenomena in photoexcited semiconductors," *Rev. Mod. Phys.* **74**(3), pp. 895–950, 2002.
4. J. Schilp, J. Kuhn, and G. Mahler, "Electron-phonon quantum kinetics in pulse-excited semiconductors: Memory and renormalization effects," *Phys. Rev. B* **50**(8), p. 5435, 1994.
5. Z. Wang, K. Reimann, M. Woerner, T. Elsaesser, D. Hofstetter, J. Hwang, W. J. Schaff, and L. F. Eastman, "Optical phonon sidebands of electronic intersubband absorption in strongly polar semiconductor heterostructures," *Phys. Rev. Lett.* **94**, p. 037403, 2005.

6. Z. Wang, K. Reimann, M. Woerner, T. Elsaesser, D. Hofstetter, E. Baumann, F. R. Giorgetta, H. Wu, W. J. Schaff, and L. F. Eastman, "Ultrafast hole burning in intersubband absorption lines of gan/aln superlattices," *Appl. Phys. Lett* **89**, p. 151103, August 2006.
7. J. Fritsch and P. Pavone, "Ab initio calculation of the structure, electronic states, and the phonon dispersion of the Si(100) surface," *Surf. Science* **344**, p. 159, 1995.
8. A. Ramstad, G. Brocks, and P. J. Kelly, "Theoretical study of the Si(100) surface reconstruction," *Phys. Rev. B* **51**, p. 14504, 1995.
9. N. Buecking, P. Kratzer, M. Scheffler, and A. Knorr, "Theory of optical excitation and relaxation phenomena at semiconductor surfaces: linking density functional and density matrix theory," *Appl. Phys. A* **88**, p. 505, 2007.
10. N. Buecking, P. Kratzer, M. Scheffler, and A. Knorr, "Linking density-functional and density-matrix theory: picosecond electron relaxation at the Si(100) surface," *submitted to Phys. Rev. Lett.* , 2007.
11. A. Zeiser, N. Bücking, J. Götte, J. Förstner, P. Hahn, W. G. Schmidt, and A. Knorr, "Dynamics of the phonon-induced electron transfer between semiconductor bulk and surface states," *Phys. Status Solidi (b)* **241**, p. R60, 2004.
12. A. Zeiser, N. Bücking, J. Förstner, and A. Knorr, "Microscopic theory of electron dynamics and time-resolved two-color two-photon photoemission at semiconductor surfaces," *Phys. Rev. B* **71**, p. 245309, 2005.
13. J. Hader, S. W. Koch, J. V. Moloney, and E. P. O'Reilly, "Influence of the valence-band offset on gain and absorption in ganas/gaas quantum well lasers," *Appl. Phys. Lett.* **76**(25), pp. 3685–3687, 2000.
14. S. Butscher, J. Förstner, I. Waldmüller, and A. Knorr, "Polaron signatures in the line shape of semiconductor intersubband transitions: quantum kinetics of the electron-phonon interaction," *Phys. Status Solidi (b)* **11**, pp. R49–R51, 2004.
15. S. Butscher, J. Förstner, I. Waldmüller, and A. Knorr, "Ultrafast electron-phonon interaction of intersubband transitions: Quantum kinetics from adiabatic following to rabi-oscillations," *Phys. Rev. B* **72**, p. 045314, 2005.
16. S. Butscher, *Many-Particle Effects in Two Dimensional Nanostructures: Semiconductor Intersubband Transitions and Graphene.* PhD thesis, Technische Universität Berlin,http://nbn-resolving.de/urn:nbn:de:kobv:83-opus-16022, 2007.
17. I. Waldmüller, J. Förstner, S.-C. Lee, A. Knorr, M. Woerner, K. Reimann, R. A. Kaindl, T. Elsaesser, R. Hey, and K. H. Ploog, "Optical dephasing of coherent intersubband transitions in a quasi-two-dimensional electron gas," *Phys. Rev. B* **69**(20), p. 205307, 2004.
18. J. Li and C. Z. Ning, "Induced transparency by intersubband plasmon coupling in a quantum well," *Phys. Rev. Lett.* **93**(8), p. 087402, 2004.
19. B. Krummheuer, V. M. Axt, and T. Kuhn, "Theory of pure dephasing and the resulting absorption line shape in semiconductor quantum dots," *Phys. Rev. B* **65**, p. 195313, May 2002.
20. J. Förstner, K. J. Ahn, J. Danckwerts, M. Schaarschmidt, I. Waldmüller, C. Weber, and A. Knorr, "Light propagation- and many-particle-induced non-Lorentzian lineshapes in semiconductor nanooptics," *Phys. Status Solidi (b)* **234**(1), pp. 155–165, 2002.
21. R. Zimmermann and E. Runge, "Dephasing in quantum dots via electron-phonon interaction," in *Proc. 26th ICPS Edinburgh*, A. R. Long and J. H. Davies, eds., *IOP Conf. Series* **171**, IOP Publishing Bristol (UK), 2002. paper M 3.1.
22. V. Meden, J. Fricke, C. Wöhler, and K. Schönhammer, "Hot electron relaxation in one-dimensional models: exact polaron dynamics versus relaxation in the presence of a fermi sea," *Z. Phys. B* , 1995.
23. S. Butscher and A. Knorr, "Theory of strong electron-phonon coupling for ultrafast intersubband excitations," *Phys. Status Solidi (b)* **243**(10), pp. 2423–2427, 2006.
24. H. Haug and S. Koch, *Quantum Theory of the Optical and Electronic Properties of Semiconductors*, World Scientific, Singapore, 2004.
25. M. Richter, T. Renger, and A. Knorr, "A bloch equation approach to intensity dependent optical spectra of light harvesting complex ii," *Photosynthesis Research* , 2007. doi:10.1007/s11120-007-9256-z.
26. S. W. Koch, N. Peyghambarian, and M. Lindberg, "Transient and steady-state optical non-linearities in semiconductors," *J. Phys. C* **21**, pp. 5229–5249, 1988.

27. S. Tanaka and K. Tanimura, "Time-resolved two-photon photoelectron spectroscopy of the Si(001)-(2×1) surface," *Surf. Science* **529**, p. 251, 2003.
28. M. Weinelt, M. Kutschera, T. Fauster, and M. Rohlfing, "Dynamics of exciton formation at the Si(100) $c(4 \times 2)$ surface," *Phys. Rev. Lett.* **92**, p. 126801, 2004.
29. P. Hohenberg and W. Kohn, "Inhomogeneous electron gas," *Phys. Rev.* **136**, p. B 864, 1964.
30. P. Rinke, A. Qteish, J. Neugebauer, C. Freysoldt, and M. Scheffler, "Combining GW calculations with exact-exchange density-functional theory: an analysis of valence-band photoemission for compound semiconductors," *New Journal of Physics* **7**, p. 126, 2005.
31. *Landolt-Börnstein*, Springer Berlin, 1987. `www.landolt-boernstein.de`.